Spatial extent of the singlet and triplet excitons in transition metal-containing poly-ynes

D. Beljonne
Cavendish Laboratory, Cambridge University, Madingley Road, Cambridge CB3 OHE, United Kingdom and Service de Chimie des Matériaux Nouveaux, Centre de Recherche en Electronique et Photonique Moléculaires, Université de Mons-Hainaut, Place du Parc 20, B-7000 Mons, Belgium

H. F. Wittmann, A. Köhler, and S. Graham
Cavendish Laboratory, Cambridge University, Madingley Road, Cambridge CB3 OHE, United Kingdom

M. Younus, J. Lewis, and P. R. Raithby
University Chemical Laboratory, Cambridge University, Lensfield Road, Cambridge CB2 EW, United Kingdom

M. S. Khan
Department of Chemistry, College of Sciences, Sultan Qaboos University, Al-Khod 123, Sultanate of Oman

R. H. Friend
Cavendish Laboratory, Cambridge University, Madingley Road, Cambridge CB3 OHE, United Kingdom

J. L. Brédas
Service de Chimie des Matériaux Nouveaux, Centre de Recherche en Electronique et Photonique Moléculaires, Université de Mons-Hainaut, Place du Parc 20, B-7000 Mons, Belgium

(Received 10 April 1996; accepted 24 May 1996)

We present a joint experimental and theoretical investigation of the electronic excitations in transition metal-containing phenylene ethynylenes. The influence of the metal on the nature of the lowest singlet and triplet excited states is characterized. We find that π conjugation occurs through the metal sites, which deeply modifies the optical properties of the conjugated chains. We also analyze the chain-length dependence of the singlet–singlet, $S_0 \rightarrow S_1$, singlet–triplet, $S_0 \rightarrow T_1$, and triplet–triplet, $T_1 \rightarrow T_n$, transition energies; both experimental data and theoretical results indicate that the lowest triplet exciton, T_1, is strongly localized on a single phenylene ring while the S_1 and T_n states extend over a few repeating units. Finally, we estimate the geometric relaxation phenomena occurring in the lowest excited states and perform a Huang–Rhys analysis of the triplet emission spectrum in model systems. © *1996 American Institute of Physics.* [S0021-9606(96)51633-8]

I. INTRODUCTION

As a result of their delocalized π-electronic wave functions, conjugated organic polymers manifest remarkable properties that make them suitable for a wide domain of applications.[1] For instance, it has been shown recently that conjugated materials can be successfully used as active layer in light emitting diodes (LEDs).[2,3] In such devices, light emission is believed to result from radiative decay of singlet excitons, created by electron-hole recombination within the organic layer;[2] triplet excitons are also produced, either by direct recombination of the charge carriers or, indirectly, through intersystem crossing from the singlet to the triplet manifold. The characterization of both the singlet and triplet excitations is thus of pivotal importance for understanding the mechanisms of LEDs based on conjugated polymers and thereby improving their characteristics.

In this context, we have recently investigated the optical properties of poly-yne derivatives including heavy metal atoms (platinum and palladium) within the conjugated backbone.[4–8] Interest in these compounds lies mainly in the large enhancement of the spin–orbit coupling induced by the heavy atoms. This coupling allows for an efficient intersystem crossing and consequently leads to a huge yield of triplet excitons (close to 100%[4]), which can then be probed more easily by conventional optical spectroscopy. The analysis of the optical response of metal-containing poly-ynes should thus provide useful insight into the characteristics of the electronic excitations in the related conjugated systems.

Besides such a fundamental aspect, this type of material may also be of interest for technological applications. For instance, highly efficient radiative recombination of triplet excitons could in principle be used to increase the efficiency of conjugated polymer-based LEDs.[4] The long lifetime and relatively high mobility of the triplet excitons in such metal-poly-yne polymers[4] allows for diffusion to dissociation centers; this gives rise to an appreciable photocurrent in photocells despite the higher binding energy of triplet excitons compared to singlet excitons.[9] By increasing the number of dissociation centers (for instance, by mixing in an electron withdrawing material such as C_{60}), we were able to improve dramatically the photocurrent quantum yield (e.g., in a photocell with a blend of Pt-poly-yne and C_{60}, photocurrent quantum yields of 1%–2% under short-circuit conditions were obtained[10]).

In this work, we first present an overview of the spec-

 0021-9606/96/105(9)/3868/10/$10.00

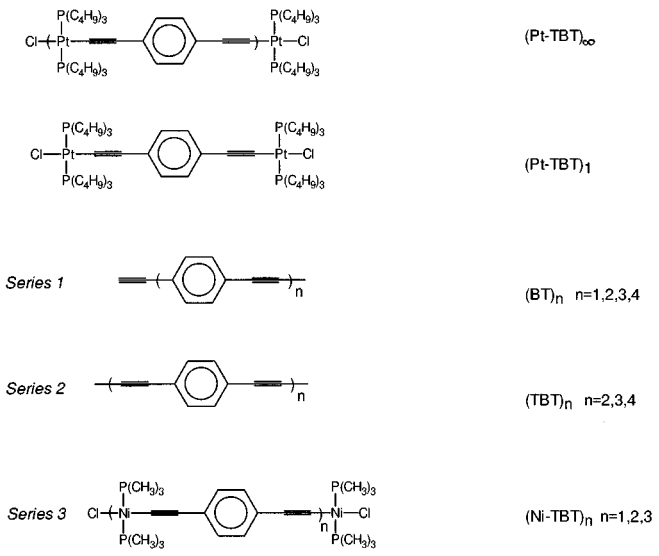

FIG. 1. Chemical structure of the compounds investigated in this work.

troscopic data accumulated on a platinum-containing poly-yne polymer, poly[*trans*(bis(tributylphosphine)Pt(1,4)phenylene–diethynylene)], and the corresponding monomer, dichloro[*trans*(bis(tributylphosphine)Pt(1,4)-phenylenediethynylene)]. The structure of these compounds are shown in Fig. 1. To unravel the nature of the lowest excited states in these systems, we have performed quantum chemical calculations on three series of molecules: (i) phenyleneethynylene oligomers (series 1); (ii) phenylenediethynylene oligomers (series 2); and (iii) *trans* (bis(trimethylphosphine)Ni(1,4)-phenylenediethynylene) oligomers (series 3), as shown in Fig. 1. Comparison of the results obtained for these three sets of calculations should allow us to obtain useful information concerning the influence on the lowest excitations of changing the number of ethynylenic units and incorporating metal atoms along the conjugated path. We also analyze the chain-length dependence of the transition energies, in order to estimate the spatial extent of the singlet and triplet excitons.

For practical reasons related to the parametrization of the technique we use, we have considered nickel rather than platinum for the compounds of series 3. Although differences in the absolute values of the electronic excitation energies can be expected when going from one metal to another, the overall description of the excited states in systems containing Ni or Pt should be rather similar, since both elements belong to the same group of the periodic table; this is supported by the fact that we observed very similar spectral features for poly-yne derivatives including platinum and palladium.[4]

The chemical structures of all compounds studied here are sketched in Fig. 1. For the sake of simplicity, we adopt the following nomenclature.[4] We abbreviate triple bonds by T and benzene rings by B; the number of repeating units is denoted by n. With this nomenclature, the platinum derivatives investigated experimentally are noted $(\text{Pt-TBT})_\infty$ for the polymer and $(\text{Pt-TBT})_1$ for the monomer; $(\text{BT})_n$, $(\text{TBT})_n$, and $(\text{Ni-TBT})_n$ refer, respectively, to the systems of series 1, 2, and 3, considered in the theoretical modeling.

Note that, in the following, we will use in an interchangeable way the terms ''exciton'' and ''excited state'' to refer to electronic excitations in conjugated systems. It should be emphasized that, *stricto sensu*, an exciton corresponds to a specific excitation in ionic solids and semiconductors, while excited states denote excitations in isolated finite chains.

II. EXPERIMENT

The platinum derivatives were synthesized according to the route described in Refs. 6 and 7. Absorption spectra were taken in dichloromethane solutions using a Perkin–Elmer λ-9 spectrophotometer. Solution concentrations were varied to allow measurements of absorption cross sections over a wide range. Photoluminescence and photoinduced absorption spectra were taken from solid thin films with absorbances of around unity at the peak of the absorption spectrum (typically 250 nm). For the photoinduced absorption measurements the platinum monomer, $(\text{Pt-TBT})_1$, was embedded in a polystyrene matrix to reduce crystallization in the solid state (M_w of polystyrene: 201 340; equal weight fractions of monomer and polystyrene). Excitation for the luminescence and photoinduced absorption measurements was made by the UV lines of an argon-ion laser (353–364 nm). The incident light was mechanically chopped and the signal recorded using a lock-in amplifier. Excitation for lifetime measurements was provided by the doubled output of a Nd:YAG-pumped dye laser (532 nm). The resonant Raman spectrum of the platinum polymer was taken at room temperature using a 457.9 nm laser line (i.e., in resonance with the singlet–triplet, $S_0 \rightarrow T_1$, excitation).

III. THEORETICAL METHODOLOGY

The ground-state geometries of compounds of series 1 and 2 are fully optimized at the Hartree–Fock semiempirical modified neglect of differential overlap (MNDO)[11] level. We build the geometries of the molecules belonging to series 3 in the following manner. For the conjugated segment, we consider the MNDO-optimized geometric parameters obtained for the oligomers of series 2. A square-planar *trans*-configuration is then adopted for the metal sites with values of 2.28, 1.82, and 2.42 Å for the Ni–P, P–C, and Ni–Cl bonds, respectively [Ref. 12, and references therein]; the Ni–C bond lengths are tuned between 1.58 and 1.88 Å to examine the influence on the excitation energies of the strength of the hybridization between the metal and the conjugated ligand orbitals. Note that x-ray measurements indicate a Ni–C bond length of ~1.85 Å in *trans*-bis(triethyl phosphine)-di(phenylethynyl)nickel.[13] It is worth stressing that the strength of the metal–ligand interaction will depend both on the nature of the metal and the distance between the metal and the conjugated bridge. From their locations in the periodic table, we can expect the following ordering of the optical gap energy in isostructural metal poly-ynes: Ni>Pd

>Pt; however, the experimental ordering is: Pd>Pt>Ni,[14] indicating a stronger interaction for nickel, that we associate to a shorter Ni–C bond.

On the basis of the optimized geometries, we perform intermediate neglect of differential overlap (INDO)[15,16]/multireference double configuration interaction (MRD-CI)[17] calculations to describe the lowest singlet and triplet excited states. The MRD-CI scheme has been detailed elsewhere.[18,19] Briefly, it consists of a two-step selection of the electronic configurations, each based on a single and double excitation configuration interaction calculation, and allows one to obtain a balanced description of the correlation effects in the ground state and in the excited states. Here, we consider two reference determinants: (i) the Hartree–Fock self-consistent-field (SCF) configuration itself; and (ii) the configuration resulting from the promotion of one electron from the highest occupied molecular orbital (HOMO) to the lowest unoccupied molecular orbital (LUMO). We have successfully applied a similar formalism to study the nature of the lowest electronic excitations in oligothiophenes.[20]

Due to strong electron–phonon coupling, lattice distortions usually occur upon photoexcitation of conjugated compounds. We have estimated the geometric relaxation effects in the poly-yne derivatives by performing geometry optimization, at the MNDO level, in the lowest singlet and triplet excited states of some compounds of series 1 and 2. In this case, the SCF procedure is conducted on the basis of a level occupancy characterized by the excitation of one electron from HOMO to LUMO; the criterion used for the geometry optimization is the excited-state energy, calculated at the CI level.

As a consequence of differences in equilibrium geometry in the ground state and in the excited state, excited-state vibrational levels can be involved in optical transitions, a feature which leads to the appearance of a vibronic structure on the optical spectra. On the basis of the information provided by Raman spectroscopy, we have performed an Huang–Rhys analysis of the triplet emission in $(\text{Pt-TBT})_\infty$ and $(\text{Pt-TBT})_1$. Assuming the Born–Oppenheimer and Franck–Condon approximations, the intensity of the vibrational sidebands is controlled by the Franck–Condon factor, which can be expressed in terms of the Huang–Rhys parameter S:

$$I(i\rightarrow j;v=0\rightarrow v=n)\propto|\langle\phi_v(i,0)|\phi_v(j,n)\rangle|^2=\frac{e^{-S_v}\times S_v^n}{n!}, \tag{1}$$

where $\phi_v(i,0)$ $[\phi_v(j,n)]$ is the vibrational function associated to the vibration normal mode v in the electronic ground state i [excited state j]. When several normal modes are involved in the same vibronic feature, the intensity of the peak is given by a product of Franck–Condon factors:

$$I(i\rightarrow j;v=0\rightarrow v=n;v'=0\rightarrow v'=m;\ldots)$$
$$\propto\frac{e^{-S_v}\times S_v^n}{n!}\,\frac{e^{-S_{v'}}\times S_{v'}^m}{m!}\cdots. \tag{2}$$

The Huang–Rhys factor, S_v, is a measure of the relative displacement of the excited-state potential energy curve with respect to the ground state along the coordinates of normal mode v; it can be estimated as

$$S_v=\frac{E_{\text{rel}}^v}{h\nu_v}, \tag{3}$$

where ν_v is the frequency of the vibration normal mode v and E_{rel}^v corresponds to the relaxation energy associated with the lattice distortions along v. The total relaxation energy with respect to a vertical excitation, E_{rel}, is then defined as the sum over all active normal modes of the contributions E_{rel}^v.

$$E_{\text{rel}}=\sum_v E_{\text{rel}}^v. \tag{4}$$

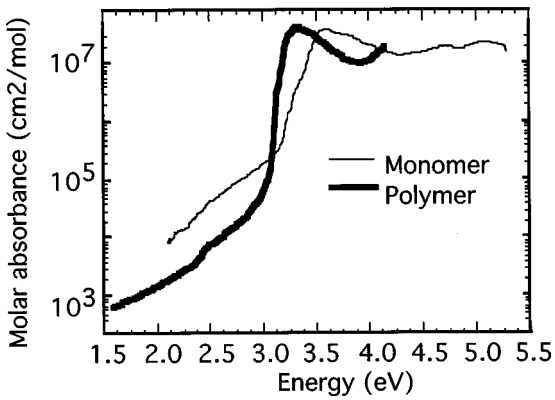

FIG. 2. Optical absorption spectra of the platinum monomer, $(\text{Pt-TBT})_1$, and polymer, $(\text{Pt-TBT})_\infty$, in dichloromethane solutions.

IV. OPTICAL SPECTROSCOPY OF THE PLATINUM–POLY-YNE DERIVATIVES

In this section, we present optical measurements for the platinum containing poly-ynes. We discuss in more detail the chain-length dependence of the optical absorption, photoluminescence, and photoinduced absorption features.

Figure 2 shows room temperature absorption spectra of solutions of the monomer $(\text{Pt-TBT})_1$ and the polymer $(\text{Pt-TBT})_\infty$ in dichloromethane. We associate the peaks in absorption at 3.59 eV for the monomer and 3.26 eV for the polymer with a singlet–singlet, $S_0\rightarrow S_1$, transition; the bathochromic shift of the absorption band with chain length clearly indicates that there is a *contact between the π orbitals of the conjugated ligand to either side of the metal*, as will be shown by our theoretical modeling in the next section. Note also that, for the polymer, a structured much weaker feature is observed at 2.43 eV, that we assign to a spin-forbidden singlet–triplet, $S_0\rightarrow T_1$ excitation; such a transition is allowed by the spin–orbit interaction mixing singlet and triplet wave functions.

Photoexcitation into the strong optical absorption band for thin films of both the Pt monomer and polymer leads to triplet emission (phosphorescence) with the 0–0 emission at 2.38 eV, which increases at low temperature (Fig. 3), as well

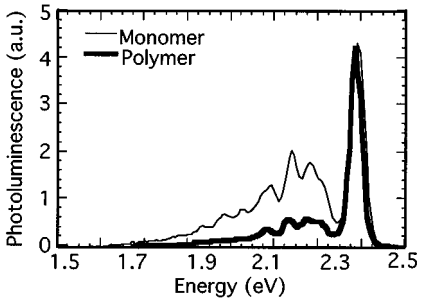

FIG. 3. Photoluminescence spectra of the platinum monomer, $(Pt\text{-}TBT)_1$, and polymer, $(Pt\text{-}TBT)_\infty$, at 30 and 10 K, respectively, from solid thin films. Excitation was provided from the UV lines of an argon–ion laser. The monomer peak intensity was scaled to match that of the polymer.

as a very structured vibronic progression; the lifetime of the emission was measured to be 44 μs for the polymer near helium temperatures and 50 μs for the monomer at 30 K. We have also measured the phosphorescence lifetime of the monomer in a polystyrene matrix to be 60 ± 10 μs. These data are consistent with a spin-forbidden transition $(T_1\rightarrow S_0)$. The very similar lifetime of the triplet excitons on the monomer in its pure form and in the polystyrene matrix indicates a low rate of bimolecular compared to monomolecular processes. The shorter lifetime of triplet excitons in the polymer might be caused by diffusion to dissociation centers along the polymer chain. Details of the temperature and time dependence of the phosphorescence signal are given elsewhere.[4] At this stage, we would like to stress that the *spectral shift of the triplet emission peak from the monomer to the polymer is extremely small* (below 0.1 eV); we conjecture that this feature is due to a strong confinement of the T_1 triplet exciton. Note also that, while singlet emission is also observed for the polymer, only the triplet excitons decay radiatively in the case of the monomer.[4]

The metastable T_1 triplet excited state, formed as a result of efficient intersystem crossing from the singlet to the triplet manifold, can be probed by photoinduced absorption (PA) measurements. The PA spectra of $(Pt\text{-}TBT)_\infty$ and $(Pt\text{-}TBT)_1$ are displayed in Fig. 4(a); these show features at 2.1 eV for the monomer and 1.49 eV for the polymer, associated to triplet–triplet, $T_1\rightarrow T_n$, transitions. The monomer spectrum shows also a long tail on the red side of the main absorption peak, which is probably due to the presence of oligomers in the sample with a distribution of conjugation lengths. We find similar temperature dependence and time evolution for the PA peaks and the triplet emission band at 2.38 eV in the polymer[4] and the monomer [Fig. 4(b)]. This supports the hypothesis that the induced absorption originates from the T_1 triplet excited state. Strikingly, the *PA band is characterized by a large red-shift (0.6 eV) when going from the monomer to the polymer*, in contrast to the situation observed for the $T_1\rightarrow S_0$ emission signal.

V. THEORETICAL MODELING OF THE EXCITED STATES IN METAL POLY-YNES

The aim of our quantum-chemical calculations is to shed light on the influence of the metal centers on the electronic

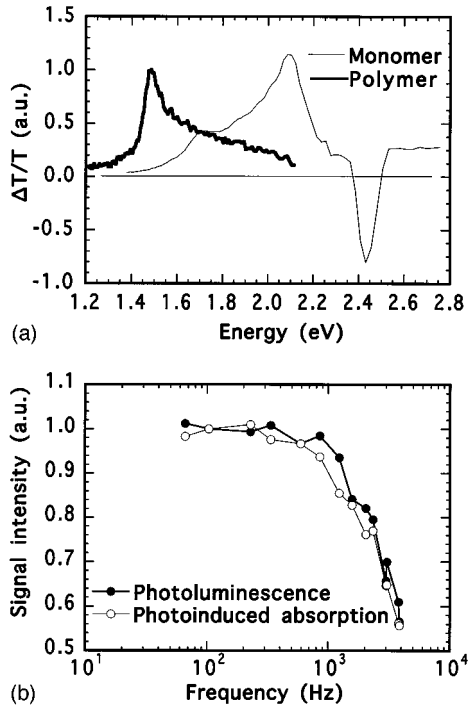

FIG. 4. (a) Photoinduced absorption spectra of the platinum monomer, $(Pt\text{-}TBT)_1$, in a polystyrene matrix and of the polymer, $(Pt\text{-}TBT)_\infty$, at 18 K, from solid thin films. (b) Chop frequency dependence of the phosphorescence and photoinduced absorption signal of the monomer in a polystyrene matrix at 20 K. The frequency dependence of the signals can be fitted using $I(\omega)=A/[(\omega^2+1/\tau^2)^{1/2}]+B$ to give a lifetime of 60 ± 10 μs. Excitation was provided from the UV lines of an argon-ion laser.

excitations and to estimate the spatial extent of the lowest singlet and triplet excited states in metal poly-yne derivatives. In Table I, we report the $S_0\rightarrow S_1$, $S_0\rightarrow T_1$, and $T_1\rightarrow T_n$ vertical excitation energies, as calculated at the INDO/MRD-CI level on the basis of the MNDO geometries for

TABLE I. INDO/MRD-CI singlet–singlet, $S_0\rightarrow S_1$ singlet–triplet, $S_0\rightarrow T_1$, and triplet–triplet, $T_1\rightarrow T_n$ excitation energies (in eV) calculated for compounds of series 1, 2, and 3; n is the number of repeating units; d (in Å) is the Ni–C bond length considered for the oligomers of series 3.

			Series 1						
n			$S_0\rightarrow S_1$			$S_0\rightarrow T_1$			$T_1\rightarrow T_n$
1			4.87			2.78			4.63
2			4.27			2.75			3.59
3			3.92			2.87			3.19
4			3.74			2.85			2.84
					Series 2				
2			4.21			2.81			3.47
3			3.96			3.02			3.23
4			3.87			(3.15)			2.68
					Series 3				
$d=$	1.88	1.73	1.58	1.88	1.73	1.58	1.88	1.73	1.58
1	4.60	4.46	4.25	3.08	3.03	2.91	3.70	3.51	3.23
2	4.56	4.21	3.61	(3.4)	(3.2)	2.89	3.39	2.97	2.54
3	4.47	4.06	3.49	(3.5)	(3.2)	2.91	3.30	2.84	2.18

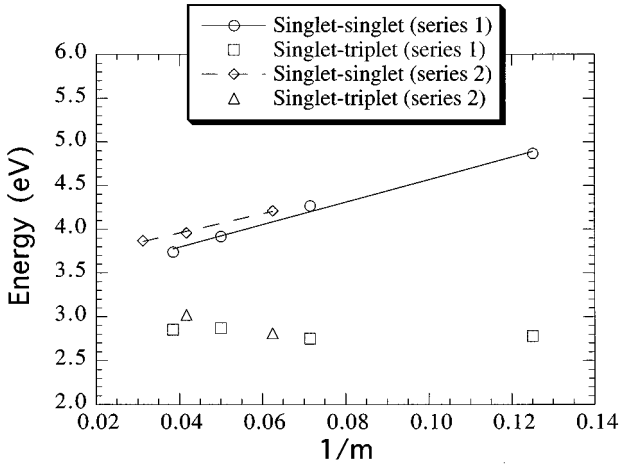

FIG. 5. Evolution with inverse chain length, $1/m$ (where m is the number of carbon atoms located on the shortest pathway between the two ends of the conjugated system), of the INDO/MRD-CI singlet–singlet, $S_0 \rightarrow S_1$, and singlet–triplet, $S_0 \rightarrow T_1$, excitation energies in compounds of series 1 and 2.

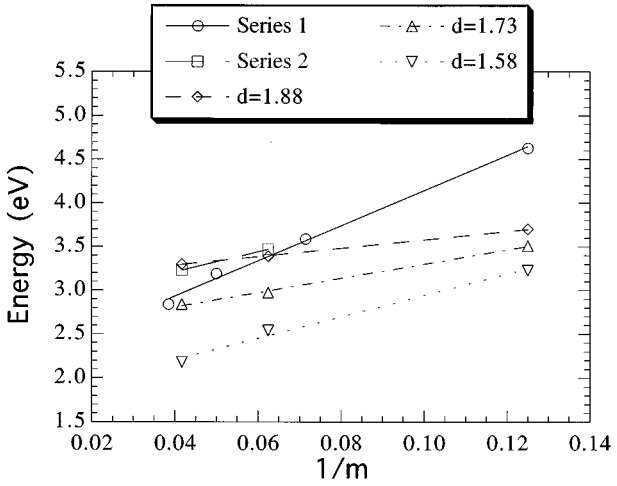

FIG. 7. Evolution with inverse chain length, $1/m$ (where m is the number of carbon atoms located on the shortest pathway between the two ends of the conjugated system), of the INDO/MRD-CI triplet–triplet, $T_1 \rightarrow T_n$, excitation energies in compounds of series 1, 2, and 3. d in the legend corresponds to the Ni–C bond length considered in the calculations.

molecules of series 1, 2, and 3; the chain-length dependence of the transition energies is illustrated in Figs. 5–7.

Focusing on the single–singlet transitions, we can point out the following observations:

(i) The singlet–singlet absorption is strongly red shifted with the number of repeating units, especially for the molecules belonging to series 1 and 2, as a result of the increase in effective conjugation length.

(ii) The comparison of the transition energies calculated for compounds of series 1 and 2 indicates that the π delocalization is reduced by the presence of triple bonds in the conjugated path; for instance, the INDO/MRD-CI $S_0 \rightarrow S_1$ excitation energies in $(BT)_3$ (3.92 eV) and $(BT)_4$ (3.74 eV) are smaller than the corresponding values in, respectively, $(TBT)_3$ (3.96 eV) and $(TBT)_4$ (3.87 eV), while the latter molecules are more extended. This is not surprising in view of the very large bond-length alternation ($\Delta r \simeq 0.15$–0.20 Å) calculated within the ethynylenic units, see Table II.

(iii) Grafting square-planar coordinated nickel sites at the ends of the $(BT)_1$ monomer induces a bathochromic displacement of the singlet–singlet, $S_0 \rightarrow S_1$, transition. As expected, the amplitude of this shift increases when shrinking the Ni–C bond length, d(Ni–C) [it amounts to 0.27 eV for d(Ni–C)=1.88 Å and to 0.62 eV for d(Ni–C)=1.58 Å].

(iv) As in the case of the molecules of series 1 and 2, we find that the $S_0 \rightarrow S_1$ excitation energies are sensitive to the number of repeating units in compounds of series 3; the slope of the curve obtained from a linear fit to the INDO/MRD-CI results increases with decreasing Ni–C bond length but is, in all cases, smaller than the one found for the related fully conjugated structures.

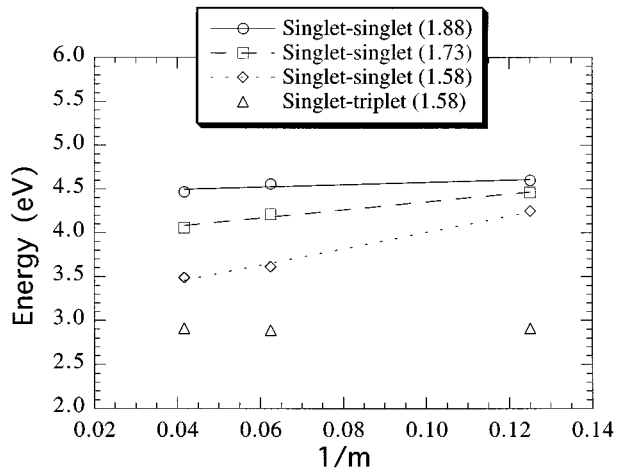

FIG. 6. Evolution with inverse chain length, $1/m$ (where m is the number of carbon atoms located on the shortest pathway between the two ends of the conjugated system), of the INDO/MRD-CI singlet–singlet, $S_0 \rightarrow S_1$, and singlet–triplet, $S_0 \rightarrow T_1$, excitation energies in compounds of series 3. The number between parentheses in the legend of the figure corresponds to the Ni–C bond length considered in the calculations.

The latter two results [(iii) and (iv)] suggest that the *nickel sites included in between the conjugated segments contribute to some delocalization of the π electrons over the whole chains, although they tend to confine the singlet excitons*. We note that similar conclusions have been drawn from preliminary extended Hückel calculations[14] and can be rationalized in the following manner. Depending on the symmetry of the molecular complex in which they are embedded, the d orbitals of the metal experience different degrees of overlap with the orbitals of the ligands and lose their original degeneracy. For a square-planar configuration, with the conjugated structure lying in the xy plane and the chain-axis oriented along x, the INDO calculations show hybridization between the $3d_{xz}$ orbitals of nickel and the π-HOMO level of the poly-yne derivative and between the Ni $4p_z$ orbitals

TABLE II. MNDO-optimized bond lengths (in Å) in the S_0 (a), S_1 (b), and T_1 (c) electronic states of some compounds of series 1 and 2. We also include the relaxation energies, E_{rel} (in eV), with respect to vertical excitations. For symmetric geometries, we only collect the parameters related to one half of the molecule.

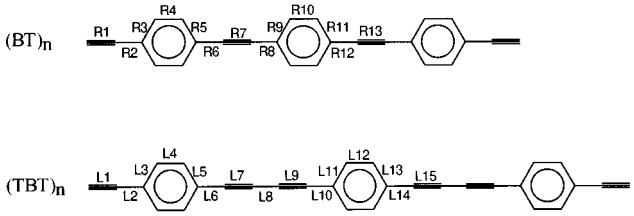

R	$(BT)_1$	$(BT)_2$	$(BT)_3$	L	$(TBT)_2$	$(TBT)_3$
(a)						
$R1$	1.198	1.198	1.198	$L1$	1.198	1.198
$R2$	1.421	1.421	1.421	$L2$	1.421	1.421
$R3$	1.417	1.418	1.417	$L3$	1.418	1.418
$R4$	1.403	1.403	1.403	$L4$	1.403	1.403
$R5$		1.418	1.418	$L5$	1.418	1.418
$R6$		1.419	1.419	$L6$	1.418	1.419
$R7$		1.202	1.202	$L7$	1.204	1.204
$R8$			1.419	$L8$	1.363	1.363
$R9$			1.418	$L9$		1.204
$R10$			1.403	$L10$		1.418
				$L11$		1.418
				$L12$		1.403
(b)						
$R1$	1.204	1.200	1.199	$L1$	1.200	1.198
$R2$	1.402	1.412	1.419	$L2$	1.415	1.423
$R3$	1.447	1.430	1.420	$L3$	1.428	1.417
$R4$	1.387	1.388	1.399	$L4$	1.390	1.400
$R5$		1.444	1.426	$L5$	1.441	1.424
$R6$		1.378	1.403	$L6$	1.382	1.402
$R7$		1.229	1.214	$L7$	1.229	1.219
$R8$			1.395	$L8$	1.330	1.337
$R9$			1.441	$L9$		1.227
$R10$			1.386	$L10$		1.377
				$L11$		1.449
				$L12$		1.379
				$L13$		
				$L14$		
				$L15$		
E_{rel}	0.12	0.21	0.17	E_{rel}	0.20	0.15
(c)						
$R1$		1.202	1.203	$L1$		1.205
$R2$		1.398	1.395	$L2$		1.394
$R3$		1.469	1.472	$L3$		1.471
$R4$		1.364	1.356	$L4$		1.358
$R5$			1.474	$L5$		1.474
$R6$			1.383	$L6$		1.385
$R7$			1.211	$L7$		1.210
$R8$			1.415	$L8$		1.367
$R9$			1.421	$L9$		1.201
$R10$			1.399	$L10$		1.420
$R11$			1.419	$L11$		1.420
$R12$			1.423	$L12$		1.401
$R13$			1.196	$L13$		1.418
				$L14$		1.422
				$L15$		1.197
E_{rel}		0.19	0.29	E_{rel}		0.31

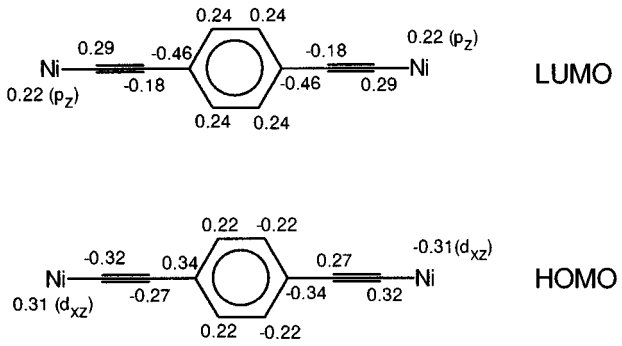

FIG. 8. INDO/MRD-CI LCAO p_z (and d_{xz}) coefficients in the HOMO and LUMO levels of the $(Ni–BT)_1$ molecule (the Ni–C distance is 1.58 Å).

and the π-LUMO level of the ligands. The frontier π orbitals are then pushed inside the original energy gap, as a result of the antibonding [bonding] character between the Ni $3d_{xz}[4p_z]$ orbitals and the HOMO [LUMO] level of the π segments; as a consequence, the first optically allowed excitation, corresponding essentially to an HOMO→LUMO π–π^* transition, is red shifted with respect to the corresponding transition in the related conjugated systems. For illustration, we present in Fig. 8 the bonding–antibonding pattern of the frontier π orbitals in the $(Ni–BT)_1$ molecule. Note also that the charge on the nickel atom is close to 2 (the calculated value, 1.587, is actually smaller as a result of back-donation effects), which is usual for a square-planar configuration.

It is interesting to point out that in all the monomers, the lowest singlet excited state is actually a charge-transfer type excited state involving molecular orbitals confined on the phenyl rings, and giving rise to a symmetry-forbidden transition to the ground state (a similar excited-state ordering has been calculated in *trans*-stilbene[21]); as a consequence, light emission through the singlet path is quenched in these systems, as is confirmed experimentally. Note that the absence of singlet emission in the platinum monomer has also to be related to the much larger quantum efficiency for triplet emission with respect to the situation prevailing in the case of the polymer. When the chain length is increased, the one-photon allowed excited state (that, for clarity, is called S_1 throughout the paper and whatever the chain length) gets more stabilized than the charge-transfer excited state and the ordering is reversed.

From Figs. 2 and 5, we have clear indications, both from the experimental data and the theoretical results, that the lowest singlet S_1 excited state is delocalized over a few repeating units. A direct comparison between the measured and calculated transition energies is difficult since differences in absolute values are expected when substituting the Pt centers by the Ni sites. By considering a Ni–C bond length of 1.58 Å, we calculate a $S_0 \rightarrow S_1$ excitation energy that amounts to 4.25, 3.61, and 3.49 eV in the monomer, dimer, and trimer, respectively; the red shift of the singlet–singlet absorption when going from the monomer to the trimer is thus close to 0.76 eV in this case. The same shift

amounts to 0.40 and 0.13 eV for Ni–C bond lengths of 1.73 and 1.88 Å, respectively. We recall that we have measured a broad optical absorption band in the Pt monomer $(Pt\text{-}TBT)_1$ that spreads from 3.5 to 4.0 eV and peaks at 3.59 eV (we conjecture that the broadness of the band is due to the presence of some polymeric impurities in the monomer); the absorption is shifted to 3.26 eV in the polymer. From the experimental absorption data, we can thus estimate the bathochromic shift between the singlet–singlet transition in the Pt monomer and polymer to be ~0.33 eV, which is consistent with the theoretical results for Ni–C bond lengths ranging between 1.73 and 1.88 Å.

Note that, in the limiting case of strong metal–ligand interaction (i.e., short Ni–C bond length), the calculated singlet–singlet transition energy is lowered by a much larger amount when going from the Ni monomer to the Ni dimer than between the dimer and trimer (for a Ni–C bond length of 1.58 Å, these energy displacements amount to ~0.7 and ~0.1 eV, respectively). We can thus estimate the *spatial extent of the S_1 singlet exciton to be close to two repeating units*; this prediction is in excellent agreement with the results of optical absorption measurements on Pt-TBT derivatives, which show very similar absorption spectra for the dimer and the polymer.[5] The good agreement between theory and experiment also allows us to rule out the possibility of an extrinsic origin (defects, impurities,...) to the finite conjugation length of the singlet exciton.

In the three series of compounds, the singlet–triplet, S_0-T_1 energy difference hardly depends on the size of the conjugated path; it stays close to 2.8–3.0 eV for all chain lengths. We note, however, that going to the longest oligomers of series 1 and 2, the S_0-T_1 excitation gets slightly blue shifted; such a shift is an artefact of the calculations and results from a poorer description of the electronic correlation effects in the longer conjugated chains. Similar effects are observed for the molecules belonging to series 3 and are amplified by increasing the Ni–C bond lengths; as the geometry of the latter compounds is not fully reoptimized after introduction of the square-planar coordinated nickel sites, we associate this effect with displacements around the equilibrium geometry on the ground-state potential energy curve.

The weak chain-length evolution of the S_0-T_1 energy difference indicates that *the lowest triplet excited state is strongly localized*; from the theoretical calculations and the measured emission spectra, we conclude that the T_1 triplet exciton is confined on a single phenylene ring. This is supported by the fact that we calculate in the n-unit oligomer of series 3, n nearly degenerate (within a 0.5 eV span) low-lying triplet excited states, characterized by a wave function involving local excitations within one of the benzene rings. We stress that the localized character of the triplet exciton has to be related to the possibility of exchange between two like-spins and is a general feature in conjugated systems, as shown by the very similar description of the T_1 excited state we have obtained in phenylene vinylene[22] and thiophene[20] oligomers. Note that the $S_0 \rightarrow T_1$ transition energy (2.8–3.0 eV) estimated from the INDO/MRD-CI calculations is in good agreement with the measured $T_1 \rightarrow S_0$ 0–0 line in emission (2.38 eV), once the substantial relaxation energy when going from the S_0 to the T_1 equilibrium geometry (on the order of 0.2–0.3 eV, see below) is taken into account.

A completely different dependence upon the size of the conjugated systems is calculated for the $T_1 \rightarrow T_n$ transition. When extending the π system, there is found to be a *very large red shift of the triplet–triplet excitation*. Actually, this energy displacement is even larger than the one found for the singlet–singlet absorption; in series 1, the bathochromic shift in the $T_1 \rightarrow T_n$ excitation when going from the monomer, $(BT)_1$, to the trimer, $(BT)_3$, amounts to ~1.8 eV, while the corresponding energy stabilization in the S_1 singlet excited state is equal to ~1.1 eV. As for the $S_0 \rightarrow S_1$ excitation, introduction of the metal sites in the conjugated path confine the triplet excitons to smaller spatial regions, which explains the smaller shift calculated for the triplet–triplet absorption in compounds of series 3 with respect to molecules of the first two series. Considering a value of 1.73 [1.58] Å for the Ni–C bond lengths, the triplet–triplet excitation energy is found to be lowered by ~0.65 [~1.05] eV between the monomer and the trimer (we recall that the corresponding displacement is close to 0.40 [0.75] eV for the singlet–singlet absorption). This description is in agreement with the experimental data extracted from linear optical and photoinduced absorption measurements on platinum poly-ynes, showing a larger redshift when going from the monomer to the polymer for the $T_1 \rightarrow T_n$ excitation (~0.6 eV) with respect to the $S_0 \rightarrow S_1$ transition (~0.4 eV). From the theoretical chain-length dependence of the triplet–triplet excitation energies, we can roughly estimate the lower bound to the size of the T_n triplet exciton to be three repeating units. It is a much larger spatial extent than the one found for the lowest triplet exciton, a feature that we rationalize by the fact that, as T_n lies at higher energy than T_1, it has a smaller binding energy and is therefore less confined; in other words, the exchange energy (defined here as the singlet–triplet energy difference), which is very large for the lowest triplet excited state [taking into account the geometric relaxation phenomena, it amounts to 1.5 and 0.8 eV in $(Ni\text{-}TBT)_1$ and $(Ni\text{-}TBT)_3$, respectively], is much smaller for higher-lying triplet excited states, which are therefore characterized by a larger spatial extent of their wave functions.

VI. GEOMETRIC RELAXATION PHENOMENA AND HUANG–RHYS FIT

The excitation energies given so far have always been calculated on the basis of the ground-state geometry. We now turn to the study of the geometric relaxation phenomena taking place in the lowest singlet, S_1, and triplet, T_1, excited states.

In Table II, we compare the MNDO-optimized geometries in the ground state, S_0, the singlet excited state, S_1, and the triplet excited state, T_1, in some model oligomers of series 1 and 2. The following conclusions can be drawn from Table II:

(i) In both the S_1 and T_1 excited states, much more pronounced lattice distortions are calculated in the ben-

zene rings than in the ethynylenic units, which appear to be extremely rigid with respect to photoexcitation.

(ii) The bond-length modifications lead to the appearance of a quinoïd geometric character on the phenylene rings, characterized by the increase in bond-length alternation, Δr (defined as the difference between the lengths of the carbon–carbon bonds orientated obliquely to the chain axis and those oriented along the chain axis), from ~0.015 Å in the ground state to ~0.06 Å in the singlet excited state, and ~0.11 Å in the triplet.

(iii) As a consequence of the rigid character of the triple bonds, the geometric defects tend to ''avoid'' the ethynylenic units and to spread out over the benzene rings, eventually leading to a breaking of the molecular symmetry; this effect is particularly strong in the T_1 triplet state of the $(BT)_2$ and $(TBT)_2$ molecules, where the geometric modifications are confined on one benzenic end-group. The lattice relaxation in the triplet T_1 excited state is thus fully consistent with a spatial extent of the triplet exciton on one phenylene unit.

(iv) The larger bond-length distortions in T_1 with respect to S_1 translate into larger relaxation energies with respect to vertical excitations (typically on the order of 0.2–0.3 eV for T_1 and 0.1–0.2 eV for S_1).

In view of the large differences between the geometric parameters in S_0 and T_1, we can expect intense vibronic sub-bands in the triplet emission spectrum of the metal poly-ynes, as seen in Fig. 3. We have fitted the vibronic structure of the phosphorescence spectra of $(Pt\text{-}TBT)_1$ and $(Pt\text{-}TBT)_\infty$ using Eqs. (1) and (2); the results are given in Fig. 9 (Gaussian functions of 0.025 eV full width at half maximum have been used to take into account both homogeneous and inhomogeneous broadenings). The frequencies of the relevant vibration normal modes have been obtained from resonant Raman spectroscopy. The Raman spectra of the Pt [Pd] polymer, measured for an excitation wavelength of 457.9 [632.8] nm (i.e., in resonance with the $T_1 \rightarrow S_0$ emission), is shown in Fig. 10 (from the strong confinement of the triplet exciton, we expect a very similar spectrum for the monomer). Note that substituting the Pt sites by Pd centers does hardly lead to any significant changes in the spectrum (see Fig. 10), which further supports the theoretical methodology adopted in this work. Four modes dominate both Raman spectra: the modes at 1166 and 2106 cm^{-1} associated to stretching of the C–C single and triple bonds; the ''breathing'' mode of the benzene rings at 1596 cm^{-1}; and a low-lying mode (839 cm^{-1}) possibly due to out-of-plane C–H vibrations (the high luminescence background is due to the spin–orbit coupling allowed $T_1 \rightarrow S_0$ transition). There is a one-to-one correspondence between the Raman peaks and the vibronic features in the triplet emission spectrum, which has allowed us to assign these features as shown in Table III; we also include in this table the normal-mode frequencies, the fitted values of the Huang–Rhys parameters, and the relaxation energy estimated on the basis of Eqs. (3) and (4)

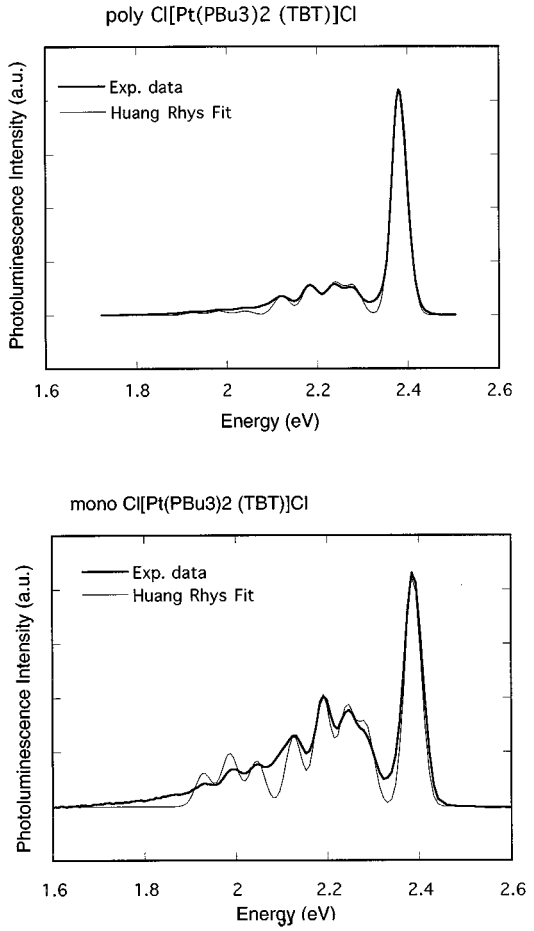

FIG. 9. Huang–Rhys fit of the photoluminescence spectra of the platinum polymer, $(Pt\text{-}TBT)_\infty$ (top panel), and monomer, $(Pt\text{-}TBT)_1$ (bottom panel).

(note that for the $T_1 \rightarrow S_0$ emission, the relaxation energy in fact corresponds to the deformation energy in the ground state when going from the S_0 to the T_1 equilibrium geometry). From Table III and Fig. 9, we see that:

(i) For both the monomer and polymer, the vibrational fit is excellent for the first four vibronic peaks but is less good at higher energy; we associate this discrepancy

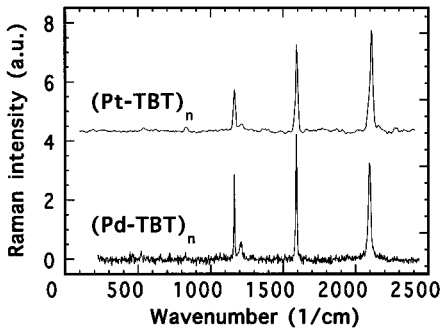

FIG. 10. Raman spectra of $(Pt\text{-}TBT)_\infty$ and $(Pd\text{-}TBT)_\infty$, measured for an excitation wavelength of 457.9 nm (Ar^+ laser) and 632.8 nm (He–Ne laser), respectively. Because of the strong luminescence, we fitted the background using high-order polynomials and substracted these from the spectra.

TABLE III. (a) Raman modes of the Pt polymer, $(Pt–TBT)_\infty$, and Huang–Rhys factors obtained by fitting the vibronic structure of the triplet emission spectra; we also include the ground-state deformation energy (in eV) when going from the S_0 to the T_1 equilibrium geometry, evaluated from Eqs. (3) and (4) ($E_d^{\exp}$) and calculated at the MNDO level (E_d^{th}). (b) Assignment of the vibronic features observed in the polymer phosphorescence spectrum (the same assignment holds true for the monomer).

(a)	Huang–Rhys factor, S_v	
Raman mode v (cm^{-1})	Monomer	Polymer
$v1=830$	0.328	0.076
$v2=1166$	0.413	0.095
$v3=1596$	0.471	0.107
$v4=2106$	0.303	0.066
$E_d^{\exp}$	0.27	0.08
E_d^{th}	0.31	...

(b) Phosphorescence feature (eV)	Offset (cm^{-1})	Assignment
2.273	839	$v1$
2.236	1137	$v2$
2.183	1565	$v3$
2.119	2081	$v4$
2.037	2742	$v3+v2$
1.987	3146	$2v3$
1.923	3662	$v3+v4$

with the presence of another excited state, with the 0–0 line close to 2.1 eV, and which has been previously assigned as a triplet dimer.[4]

(ii) The global ground-state deformation energy (0.27 eV) associated with distortions from the S_0 to T_1 equilibrium geometry in $(Pt-TBT)_1$ is in excellent agreement with the value calculated at the MNDO level (0.31 eV); in the Pt polymer, the deformation energy is much lower (0.08 eV) and the vibronic intensity is strongly reduced, which suggests a flattening of the ground-state potential energy curve when increasing the chain length.

VII. CONCLUSIONS

We have performed a joint experimental and theoretical analysis of the lowest singlet and triplet excited states in metal-containing poly-yne derivatives. Hybridization occurs between the metal d orbitals and the p_z orbitals of the ligands, which strongly modifies the optical response of the conjugated chains. The chain-length dependences of the singlet–singlet, $S_0 \rightarrow S_1$, singlet–triplet, $S_0 \rightarrow T_1$, and triplet–triplet, $T_1 \rightarrow T_n$, excitation energies, as obtained from various spectroscopic techniques and as calculated by the INDO/MRD-CI scheme are consistent with a spatial extent of roughly one and two repeating units for the T_1 and S_1 excited states, respectively, while the T_n wave function spreads out over at least three units. The Huang–Rhys analysis of the triplet emission spectrum of model systems indicates that significant and local lattice distortions take place in the lowest triplet excited state, as confirmed by a theoretical modeling of the geometric relaxation phenomena.

Besides their great potential for technological applications, materials in which the triplet states are more easily accessible, such as metal poly-ynes derivatives, are of fundamental interest in understanding the nature of the lowest excited states in conjugated polymers, such as *poly*(*p*-phenylene vinylene)s (PPV), intensively investigated for their light emission properties.[2,3] In this context, the overall description provided by the study of metal poly-yne derivatives is consistent with the formation of excitons as the primary photoexcited species in light-emitting conjugated polymers, in that the lowest singlet and triplet excitations in these materials are confined on a few repeating units. The exact spatial extent of the excitons of course depends both on the spin multiplicity of the excited species and on the chemical structure of the conjugated chain and can be related to the binding energy; the larger the binding energy, the stronger the confinement of the excited state wavefunction. In PPV, the rather small binding energy (on the order of 0.1–0.4 eV[23]) is consistent with a singlet S_1 exciton that spreads out over a spatial domain on the order of 5 phenylene rings.

Moreover, as the T_1 triplet exciton is localized on one phenylene ring in the Pt poly-ynes compounds, and assuming that the same description holds true in poly(paraphenylene vinylene), we can estimate the S_0-T_1 energy difference in PPV from the triplet emission energy (2.38 eV) measured for the transition metal-containing polymer. However, this value should be regarded as an upper bound, since in PPV, the vinylene linkages are expected to be preferential sites for the accommodation of the excited species. From similar INDO/MRD-CI calculations on PPV oligomers,[22] we have extrapolated the T_1 excited state to be $\sim$0.6 eV below the S_1 excited state in the polymer; assuming a value of $\sim$2.4 eV for the singlet–singlet transition, this would place the lowest triplet in PPV at $\sim$1.8 eV above the ground state.

ACKNOWLEDGMENTS

This work is partly supported by the Belgian Federal Government Office of Science Policy (SSTC) ''Pôle d'Attraction Interuniversitaire en Chimie Supramoléculaire et Catalyse,'' Fonds National Belge de la Recherche Scientifique (FNRS), an IBM-UMH Academic Joint Study, the UK Engineering and Physical Sciences Research Council, and Human Capital and Mobility Network ''SELMAT.'' One of us (D.B.) is Chargé de Recherche FNRS. The authors thank Professor M. Zerner for the ZINDO package and stimulating discussions.

[1] *Handbook of Conducting Polymers*, edited by T. Skotheim (Marcel Dekker, New York, 1986), Vols. 1 and 2; *Conjugated Polymers: The Novel Science and Technology of Highly Conducting and Nonlinear Optically Active Materials*, edited by J. L. Brédas and R. Silbey (Kluwer, Dordrecht, 1991).

[2] J. H. Burroughes, D. D. C. Bradley, A. R. Brown, R. N. Marks, K. McKay, R. H. Friend, P. L. Burn, and A. B. Holmes, Nature (London) **347**, 539 (1990); P. L. Burn, D. D. C. Bradley, A. R. Brown, R. N. Marks, K. McKay, R. H. Friend, P. L. Burn, and A. Kraft, J. Chem. Soc., Perkin Trans. 3225 (1992).

[3] D. Braun and A. J. Heeger, Appl. Phys. Lett. **58**, 1982 (1991).

[4] H. F. Wittmann, R. H. Friend, M. S. Kahn, and J. Lewis, J. Chem. Phys. **101**, 2693 (1994); H. F. Wittmann and R. H. Friend (unpublished).

[5] H. F. Wittmann, Ph.D. thesis (Cambridge, 1993).
[6] B. F. G. Johnson, A. K. Kakkar, M. S. Kahn, J. Lewis, A. E. Dray, R. H. Friend, and F. Wittmann, J. Mater. Chem. **1**, 485 (1991).
[7] J. Lewis, M. S. Kahn, A. K. Kakkar, B. F. G. Johnson, T. B. Marder, H. B. Fyfe, F. Wittmann, R. H. Friend, and A. E. Dray, J. Organomet. Chem. **425**, 165 (1992).
[8] A. E. Dray, R. Rachel, W. O. Saxton, J. Lewis, M. S. Kahn, A. M. Donald, and R. H. Friend, Macromolecules **25**, 3473 (1992).
[9] A. Köhler, H. F. Wittmann, R. H. Friend, M. S. Khan, and J. Lewis, Synth. Met. **67**, 245 (1994).
[10] A. Köhler, H. F. Wittmann, R. H. Friend, M. S. Kahn, and J. Lewis, Synth. Met. (in press).
[11] M. J. S. Dewar and W. Thiel, J. Am. Chem. Soc. **99**, 4899 (1977).
[12] E. M. Graham, V. M. Miskowski, J. W. Perry, D. R. Coulter, A. E. Stiegman, W. P. Stiegman, W. P. Schoefer, and R. E. Marsh, J. Am. Chem. Soc. **111**, 8771 (1989).
[13] G. R. Davies, R. H. B. Mais, and P. G. Owston, J. Chem. Soc. 1750 (1967).
[14] O. Lhost, J. M. Toussaint, J. L. Brédas, H. F. Wittmann, K. Fuhrmann, R. H. Friend, M. S. Kahn, and J. Lewis, Synth. Met. **55–57**, 4525 (1993).
[15] J. Ridley and M. Zerner, Theoret. Chim. Acta **32**, 111 (1973).
[16] Z. S. Herman, R. F. Kirchner, G. H. Loew, U. T. Mueller-Westerhoff, A. Nazzal, and M. Zerner, Inorg. Chem. **21**, 46 (1982).
[17] R. J. Buenker and S. D. Peyerimhoff, Theoret. Chim. Acta **35**, 33 (1974).
[18] P. Tavan and K. Schulten, J. Chem. Phys. **85**, 6602 (1986); Phys. Rev. B **36**, 4337 (1987).
[19] Z. Shuai, D. Beljonne, and J. L. Brédas, J. Chem. Phys. **97**, 1132 (1992).
[20] D. Beljonne, J. Cornil, R. H. Friend, R. A. J. Janssen, and J. L. Brédas, J. Am. Chem. Soc. (in press).
[21] Z. G. Soos, S. Ramasesha, D. S. Galvao, and S. Etemad, Phys. Rev. B **47**, 1742 (1993).
[22] D. Beljonne, Z. Shuai, R. H. Friend, and J. L. Brédas, J. Chem. Phys. **102**, 2042 (1995).
[23] J. L. Brédas, J. Cornil, and A. J. Heeger, Adv. Mater. **8**, 447 (1996).